The Synthesis, Structural Analysis and Magnetic Properties of a New Mixed Metal Ferrite $Ba_3Fe_{24}Ti_7O_{53}$

Richard D. Adams*[a], Ralph Layland[a], and Christophe Payen*[b]

Department of Chemistry and Biochemistry[a],
University of South Carolina, Columbia, SC 29208, U.S.A.
Telefax: (internat.) +8037776781
E-mail: Adams@psc.sc.edu

Institut des Matériaux de Nantes[b],
2 rue de la Houssinière, F-44072 Nantes Cedex 03, France

Received May 29, 1996

Key Words: Ferrite / Iron oxide / Titanate

A new mixed metal titanate $Ba_3Fe_{24}Ti_7O_{53}$, **1** was obtained by heating stoichiometic mixtures of $BaCO_3$, Fe_3O_4 and TiO_2 to 1375 °C for 48 h. Compound **1** was characterized by single crystal x-ray diffraction analysis. Two of the barium ions lie in a network of channels in the *bc* crystallographic plane. The iron and titanium atoms were refined in a random distribution in 16 independent MO_6 octahedral sites and 2 MO_4 tetrahedral sites. Magnetization measurements reveal a strong magnetic ordering up to 600 K. M vs. H loop measurements show no hysteresis effects.

Introduction

Due to their strong ferrimagnetic ordering, ferrites have been found to be useful for a variety of electronic applications ranging from magnetic recording devices[1] to the cores of power transformers[2]. "Soft" ferrites, such as $MnFe_2O_4$ and $NiFe_2O_4$, are of particular interest for use as cores in inductors and in pulse and wide band transformers because they exhibit little or no magnetic hysteresis[2]. $BaFe_{12}O_{19}$ is a well studied "hard" ferrimagnet[2]. Efforts to reduce the intrinsic magnetic hysteresis in $BaFe_{12}O_{19}$ have induced varying the particle sizes and isomorphous replacement of some of the iron with magnetically less-responsive elements, such as cobalt and titanium[3]. Attempts to replace the iron in $BaFe_{12}O_{19}$ with other metals have also led to the formation of some new mixed metal phases[4–6].

Recently, we have been investigating the solid state reactions of $BaCO_3$ with mixtures of TiO_2 and oxides of nickel and iron and have obtained two isomorphous mixed metal oxides, $BaNiTi_5O_{13}$[7] and $BaFe_2Ti_4O_{13}$[4b]. In further studies of the Ba/Fe/Ti/O system we have now obtained a new phase that we have identified as $Ba_3Fe_{24}Ti_7O_{53}$. The results of our studies of the synthesis, crystal structure analysis and magnetic properties of $Ba_3Fe_{24}Ti_7O_{53}$, **1** are reported here.

Results and Discussion

The new compound $Ba_3Fe_{24}Ti_7O_{53}$, **1** was obtained by heating a mixture of $BaCO_3$, Fe_3O_4 and TiO_2 in the stoichiometric ratio to 1375 °C for 48 h. The dark brown material was shown pure by x-ray diffraction analysis of the powder form, but could contain up to 5% impurity by this test. Details of the crystal structure were obtained by single crystal x-ray diffraction analysis (see Table 1). The structure was solved in the centric space group *C2/m*. Selected interatomic distances are listed in Table 2. The three independent barium ions occupy the special positions: *4g*, *4h* and *4i*. Each

Table 1. Crystallographic data

Formula	$Ba_3Fe_{24}Ti_7O_{53}$
Formula weight	2935.59
Crystal system	Monoclinic
Lattice parameters	
a (Å)	19.416(4)
b (Å)	20.280(4)
c (Å)	10.080(2)
α (°)	90.00
β (°)	105.38(1)
γ (°)	90.00
V (Å^3)	3826.9(1)
Space group	*C2/m* (No. 12)
Z value	4
$\rho_{calc.}$ (g/cm^3)	5.09
μ (Mo Kα) (cm^{-1})	133.32
Temperature (°C)	20
2Θmax (°)	55
No. Obs. (I>3σ)	3153
No. Variables	277
Goodness of Fit (GOF)	2.18
Residuals: R; R_w	0.048; 0.049
Abs. Cor. (based on 3 azimuthal psi scans)	empirical
Transmission coeff. Max/Min	1.00/0.502
Largest peak in Final Diff. Map (e$^-$/Å^3)	2.70

$R = \Sigma_{hkl}(||F_{obs}| - |F_{calc}||)/\Sigma_{hkl} |F_{obs}|$;
$R_w = [\Sigma_{hkl} w(|F_{obs}| - |F_{calc}|^2)/\Sigma_{hkl} w F_{obs}^2]^{1/2}$,
$w = 1/\sigma^2(F_{obs})$;
$GOF = [\Sigma_{hkl}(w|F_{obs}| - |F_{calc}|)^2/(n_{data} - n_{vari})]^{1/2}$

  0009–2940/96/1212–1441 $ 15.00+.25/0

barium ion contains twelve nearest neighbours in the usual cubic close-packed arrangement. All Ba–O contacts lie within the range: 2.827(8) Å–3.07(1) Å. The transition metal ions occupy 18 independent sites in the solid state structure. Five of these metal containing sites are special positions, all *4i* (having *m* symmetry); the remainder lie in general positions. From this total, the metal composition in the formula was established as 31. There are 33 independent oxide containing sites, eight of these are special positions (see Table 2). This allowed the total oxygen composition to be determined as 53 oxides. By assuming that all iron was present in the +3 oxidation state and all titanium was present in the +4 oxidation state, the relative transition metal composition, $Fe_{24}Ti_7$, was determined by charge balance. The $Ba_3Fe_{24}Ti_7$ composition was subsequently confirmed by electron microprobe analysis. Attempts to refine the relative Fe/Ti occupancy in the metal sites showed no significant deviations from the random (completely disordered) state. Accordingly, this result was used in the final analysis (i.e. all transition metal sites were refined containing 24/31 th iron and 7/31 th titanium). However, it is possible that the quality of the data were simply insufficient to reveal deviations from the nonrandom state, since the difference in the x-ray scattering power between iron and titanium is not large. In studies of other barium iron titanates nonrandom distributions of iron and titanium have been found[4b]. For sixteen of the 18 transition metal sites, the metal ions are surrounded by six oxide ions in the octahedral geometry. For two of the metal sites, M(3) and M(4), the metal ions have only four oxide neighbors which are arranged in a tetrahedral geometry.

A view of the two adjacent unit cells of the crystal lattice of **1** which have the *ab* plane in common is shown in Figure 1. The *ab* plane is shown in the forefront of the figure with the *bc* plane in perspective along the top. The barium ions are represented as circles containing a number that corresponds to its lattice site. Ions Ba(1) and Ba(2) lie in channels in the *bc* plane. Ba(3) lies in the *ac* plane. The transition metal sites are represented as polyhedra, octahedra (gray) and tetrahedra (darkened). The tetrahedral site M(3) lies in the *ac* plane and is clearly visible at the sides of the *ab* plane.

The connectivity of the metal polyhedra is shown in the four sections of the unit cell, Figures 2–5, which show half the unit cell in four layers perpendicular to the a^* direction over the range, $a = 0.0–0.5$. The top section, Figure 2, shows the network of channels containing the barium ions Ba(1) and Ba(2) (circles) and their relationship to the edge-fused octahedra in the layer of metal atoms lying between $a = 0.0–0.16$. Triangular M_6 clusters lie at the corners of the cell. A large M_9 triangle of octahedra (four octahedra on each edge with an empty cavity in the center) occupies the center of the cell. This large grouping is linked to similar neighboring groups to form an extended chain in the *c* di-

Table 2. Interatomic distances [Å] for **1**

Ba(1) O(8) 2.99(1)	M(6) O(12') 2.128(8)	Ba(2) M(6) 3.737(2)	M(12) O(33) 2.000(8)
Ba(1) O(10) 2.836(8)	M(6) O(19) 1.919(8)	Ba(2) M(13) 3.527(2)	M(13) O(16) 2.249(8)
Ba(1) O(10') 2.836(8)	M(6) O(25) 1.976(8)	Ba(2) M(15) 3.434(2)	M(13) O(18) 2.218(3)
Ba(1) O(18) 2.98(1)	M(6) O(33) 2.019(8)	Ba(2) M(17) 3.465(3)	M(13) O(23) 1.899(8)
Ba(1) O(22) 2.964(8)	M(7) O(1) 1.942(8)	Ba(3) M(3) 3.589(3)	M(13) O(25) 1.926(8)
Ba(1) O(22') 2.964(8)	M(7) O(4) 2.002(8)	Ba(3) M(4) 3.517(2)	M(13) O(27) 2.072(8)
Ba(1) O(23) 2.881(8)	M(7) O(20) 2.185(8)	Ba(3) M(9) 3.589(2)	M(13) O(30) 1.900(9)
Ba(1) O(23) 2.881(8)	M(7) O(20') 2.098(8)	Ba(3) M(14) 3.719(3)	M(14) O(6) 1.916(8)
Ba(1) O(24) 2.837(8)	M(7) O(23) 1.942(8)	Ba(3) M(16) 3.635(3)	M(14) O(6') 1.916(8)
Ba(1) O(24') 2.837(8)	M(7) O(24) 2.066(8)	Ba(3) M(18) 3.664(2)	M(14) O(7) 2.113(8)
Ba(1) O(30) 2.897(8)	M(8) O(10) 1.925(8)	M(1) O(8) 2.075(8)	M(14) O(7') 2.113(8)
Ba(1) O(30') 2.897(8)	M(8) O(12) 2.042(8)	M(1) O(8') 2.075(8)	M(14) O(9) 1.90(1)
Ba(2) O(5) 2.827(8)	M(8) O(19) 1.920(8)	M(1) O(21) 1.958(8)	M(14) O(17) 2.09(1)
Ba(2) O(5') 2.827(8)	M(8) O(20) 2.164(8)	M(1) O(21') 1.958(8)	M(15) O(14) 1.891(8)
Ba(2) O(14) 2.863(8)	M(8) O(23) 2.063(8)	M(1) O(28) 1.99(1)	M(15) O(14') 1.8918)
Ba(2) O(14') 2.863(8)	M(8) O(33) 2.055(8)	M(1) O(29) 1.99(1)	M(15) O(15) 2.12(1)
Ba(2) O(16) 2.984(8)	M(9) O(4) 1.984(8)	M(2) O(6) 1.974(8)	M(15) O(16) 2.226(8)
Ba(2) O(16') 2.984(8)	M(9) O(10) 2.006(8)	M(2) O(8) 2.072(2)	M(15) O(16') 2.226(8)
Ba(2) O(25) 2.876(8)	M(9) O(20) 2.102(8)	M(2) O(10) 1.939(8)	M(15) O(32) 1.911(3)
Ba(2) O(25') 2.876(8)	M(9) O(21) 1.849(8)	M(2) O(22) 2.062(8)	M(16) O(2) 2.273(3)
Ba(2) O(30) 2.938(8)	M(9) O(24) 1.997(8)	M(2) O(28) 2.033(7)	M(16) O(3) 1.84(1)
Ba(2) O(30') 2.938(8)	M(9) O(26) 2.031(8)	M(2) O(29) 2.216(8)	M(16) O(16) 2.014(8)
Ba(2) O(31) 2.96(1)	M(10) O(6) 1.967(8)	M(3) O(17) 1.86(1)	M(16) O(16') 2.014(8)
Ba(2) O(32) 2.853(1)	M(10) O(11) 2.053(8)	M(3) O(26) 1.863(8)	M(16) O(27) 1.942(8)
Ba(3) O(4) 2.947(8)	M(10) O(13) 1.971(8)	M(3) O(26') 1.863(8)	M(16) O(27') 1.942(8)
Ba(3) O(4') 2.947(8)	M(10) O(19) 1.874(8)	M(3) O(28) 1.89(1)	M(17) O(5) 1.907(8)
Ba(3) O(7) 2.923(8)	M(10) O(22) 1.982(8)	M(4) O(4) 1.871(8)	M(17) O(13) 2.126(8)
Ba(3) O(7') 2.923(8)	M(10) O(31) 2.052(8)	M(4) O(7) 1.868(8)	M(17) O(22) 2.154(8)
Ba(3) O(9) 3.07(1)	M(11) O(9) 1.953(8)	M(4) O(12) 1.878(8)	M(17) O(24) 1.907(8)
Ba(3) O(15) 2.89(1)	M(11) O(11) 2.021(3)	M(4) O(13) 1.903(8)	M(17) O(30) 1.866(9)
Ba(3) O(21) 3.034(8)	M(11) O(13) 2.029(8)	M(5) O(3) 1.963(7)	M(17) O(31) 2.221(3)
Ba(3) O(21') 3.034(8)	M(11) O(21) 2.026(8)	M(5) O(7) 1.949(8)	M(18) O(1) 1.861(8)
Ba(3) O(26) 2.960(8)	M(11) O(22) 2.114(8)	M(5) O(14) 2.141(8)	M(18) O(2) 2.241(2)
Ba(3) O(26') 2.960(8)	M(11) O(29) 2.072(8)	M(5) O(17) 2.063(8)	M(18) O(15) 1.945(7)
Ba(3) O(27) 2.871(7)	M(12) O(1) 1.932(8)	M(5) O(25) 1.964(8)	M(18) O(16) 1.998(8)
Ba(3) O(27') 2.871(7)	M(12) O(5) 2.089(8)	M(5) O(33) 2.058(8)	M(18) O(18) 2.015(6)
Ba(1) M(2) 3.451(2)	M(12) O(14) 1.934(8)	M(6) O(5) 1.966(8)	M(18) O(27) 1.944(8)
Ba(1) M(13) 3.470(2)	M(12) O(20) 2.212(8)	M(6) O(12) 2.018(8)	
Ba(1) M(17) 3.428(2)	M(12) O(26) 1.995(8)		

Figure 1. A perspective view of two unit cells of the solid state structure of $Ba_3Fe_{24}Ti_7O_{53}$, **1** showing the *ab* plane in the foreground and *bc* plane along the top; the MO_6 and MO_4 groups are represented as polyhedra; the barium ions are represented by the circles

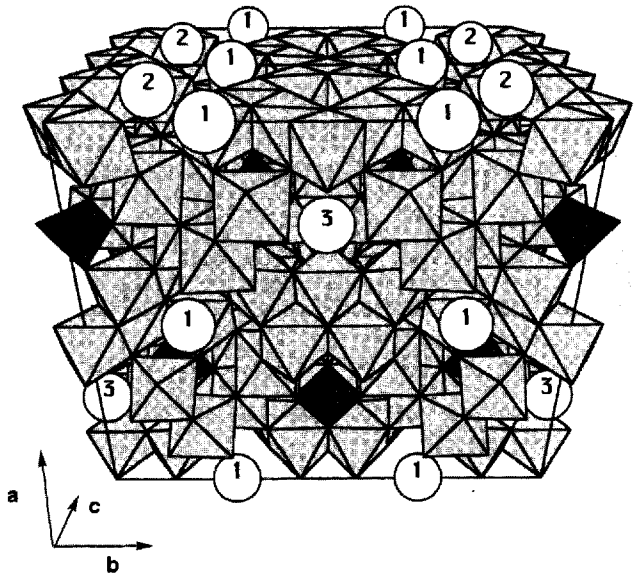

rection by two edges of an MO_6 octahedron at one of the vertices. Vertical symmetry planes lie in the *ac* plane along each side and thorough the center of the figure.

Figure 2. A view of a section of the unit cell of the structure of $Ba_3Fe_{24}Ti_7O_{53}$, **1** parallel to the *bc* plane over the range $a = 0.00-0.016$; the MO_6 groups are represented as polyhedra; barium ions are represented by the circles; the solid lines represent the cell boundary

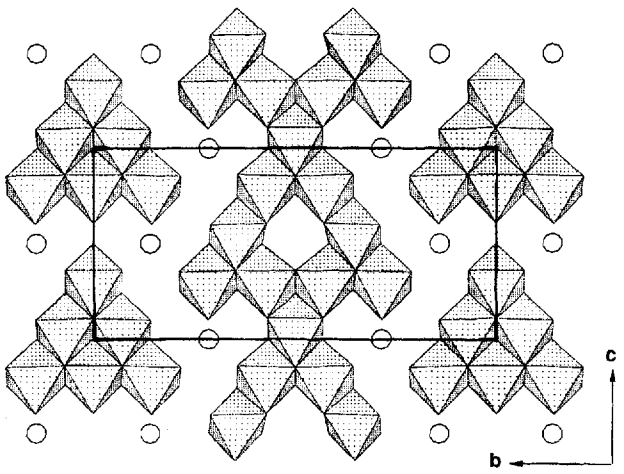

The second layer, Figure 3, $a = 0.16-0.31$ shows the location of the barium ions Ba(3), all of the symmetry related tetrahedral sites and some additional octahedral sites. Each barium ion is surrounded by a triangular grouping three proximate tetrahedra that are linked by neighboring vertices of a single MO_6 octahedron. The tetrahedra surrounding the Ba(3) ions in the *ac* plane face the viewer. Those surrounding the Ba(3) ions at $b = 0.5$ face away from the viewer.

Figure 3. A view of a section of the unit cell of the structure of **1** parallel to the *bc* plane over the range $a = 0.16-0.031$; the MO_6 and MO_4 groups are represented as polyhedra; barium ions are represented by the circles; the solid lines represent the cell boundary

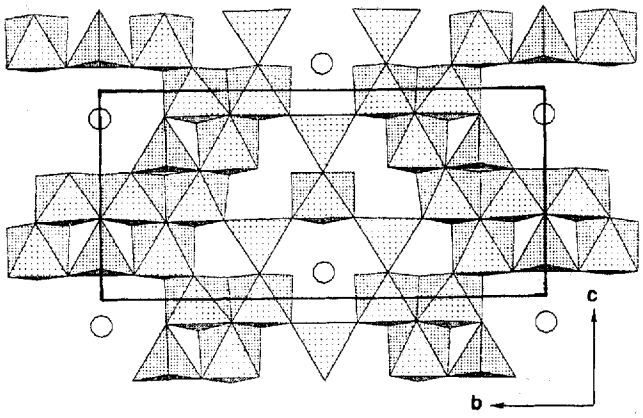

Figure 4 and 5 show the location of edge-shared MO_6 octahedra in the layers, $a = 0.31-0.43$ and $a = 0.43-0.56$, respectively. The barium ions represented in Figure 5 are the same one as shown in Figure 2, but are displaced 0.5 of a unit translation in the *b* direction due to the *C*-centering of the lattice. Likewise, the entire structure in the range $a = 0.50-0.66$ is identical to that in the $a = 0.00-0.16$ range with a displacement of 0.5 of a unit translation in the *b* direction due to the *C*-centering of the lattice.

Figure 4. A view of a section of the unit cell of the structure of $Ba_3Fe_{24}Ti_7O_{53}$, **1** parallel to the *bc* plane over the range $a = 0.31-0.043$; the MO_6 groups are represented as polyhedra

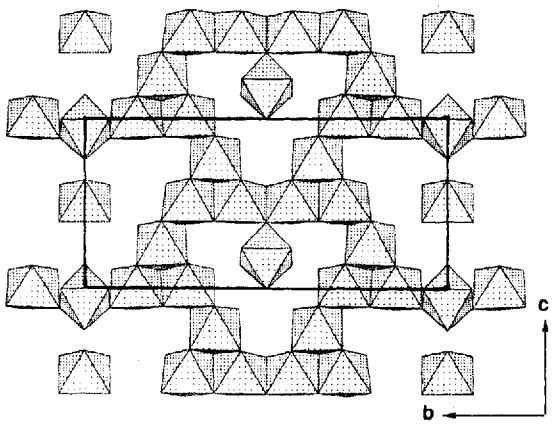

Figure 6 shows the temperature dependence of the ratio of the magnetization *M* to the applied field, *H*, for a ZFC/FC set of measurements at $H = 500$ Oe. The compound exhibits paramagnetic behavior only above 600 K. Unfortunately, the data in the range 600–700 K are not sufficient to allow the calculation of an effective magnetic moment per formula unit. At temperatures below 600 K, both the ZFC (O) and FC (+) curves show a sharp increase followed by a plateau. This is probably due to a ferrimagnetic ordering in this region. An *M* vs. *H* loop measurement at 290

Figure 5. A view of a section of the unit cell of the structure of $Ba_3Fe_{24}Ti_7O_{53}$, **1** parallel to the *bc* plane over the range $a = 0.43-0.056$; the MO_6 groups are represented as polyhedra; the barium ions are represented by the circles

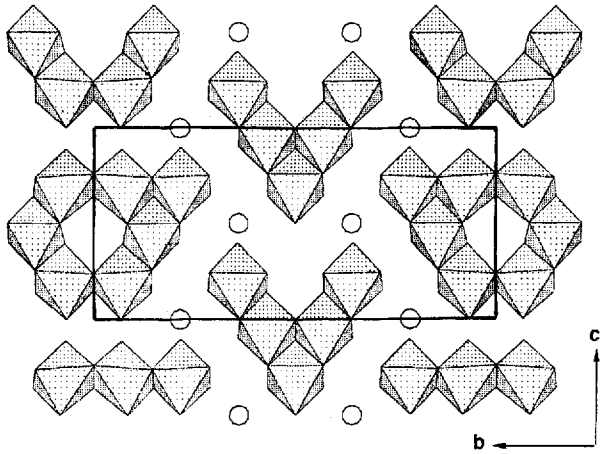

K shows that saturation is reached at about 10 kOe and that there is virtually no detectable hysteresis (see Figure 7). This feature is characteristic of "soft" ferrimagnets[1,2] and is quite different from that of $BaFe_{12}O_{19}$ which exhibits a substantial hysteresis and magnetic anisotropy[2,8].

Figure 6. Plots of magnetization M/H versus temperature (K) for compound **1**; (○) Zero Field Cooled measurements, (+) Field Cooled measurements

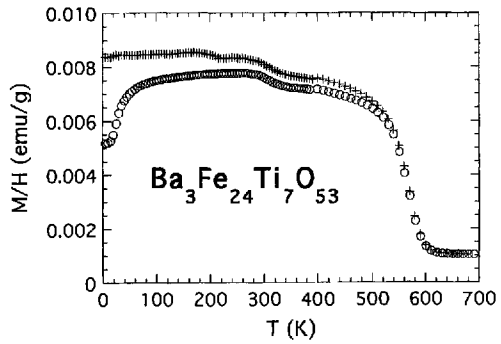

Figure 7. Magnetization vs. field (H) loop plots between −20 and +20 kOe measured at $T = 290$ K for compound **1**

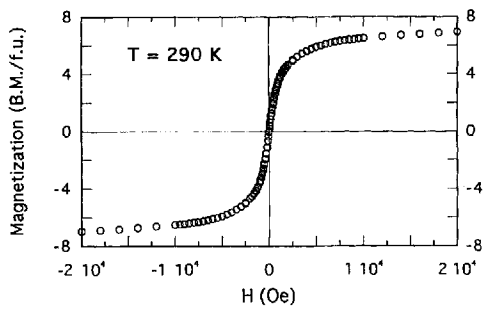

Magnetic hysteresis in ferro- and ferrimagnetic materials is a result of resistance to reversal of the ordered magnetic state when an applied field is reversed, and is attributed to resistance in the movement of the magnetic domain walls through the crystal (i.e. domain wall dynamics)[1]. This is generally attributed to the magnetocrystalline anisotropy of the material, but crystal imperfections which can block wall movement and/or nucleate new reverse field domains and even the physical shape of the crystal are also known to be important[1,2]. Details concerning the explanation of the very small hysteretic effects found in **1** will require additional studies.

We thank Dr. *Neil Summer* for performing the electron microprobe analyses.

Experimental

The reagents $BaCO_3$ (99.98%), Fe_3O_4 (98%) and TiO_2 (99.9%) were purchased from Aldrich. These were used without further purification. The reaction mixtures were heated in a Thermolyne Model F46120CM oven in an atmosphere of air. Diffraction measurements were made on a Rigaku AFC6S automatic diffractometer by using graphite-monochromated Mo-K_α radiation. Metal composition measurements were obtained on a single crystal of the compound by electron microprobe analysis performed at the University of South Carolina by using a Cameca SX-50 electron microprobe analyzer with wavelength dispersion.

Synthesis and Characterization of $Ba_3Fe_{24}Ti_7O_{53}$: A mixture of 0.326 g (1.65 mmol) of $BaCO_3$, 1.018 g (4.39 mmol) of Fe_3O_4, and 0.309 g (3.87 mmol) of TiO_2 was ground thoroughly in a mortar, and then transferred to a platinum crucible. The platinum crucible was placed in the oven and heated to 1375 °C for 48 h. After this period, the oven was cooled slowly (approx. 1 °C/min) to 1000 °C, then allowed to cool rapidly to room temperature. The crucible was removed from the oven at room temperature. An x-ray powder analysis indicated that the bulk of the sample was the material $Ba_3Fe_{24}Ti_7O_{53}$ in a pure form. – Analysis: relative % composition Ba:Fe:Ti calcd. 20:64:16; found 20:62:18.

Crystallographic Analyses: Single crystals of **1** suitable for x-ray diffraction analysis were cleaved from the bulk material in the crucibles in which the preparations were carried out. A dark brown crystal of **1** was cleaved from the bulk sample by using a scalpel. The crystal used for the intensity measurements was mounted in a thin-walled glass capillary. The unit cell was determined from 15 randomly selected reflections obtained by using the AFC6 automatic search, center, index, and least-squares routines. Crystal data, data collection parameters, and results of the analysis are listed in Table 1. All data processing was performed on a Silicon Graphics INDIGO2 computer by using the TEXSAN structure solving program library obtained from the Molecular Structure Corp., The Woodlands, TX. Lorentz-polarization (Lp) and an absorption correction (based on three azimuthal psi scans) were applied to all of the data. Neutral atom scattering factors and anomalous dispersion corrections were applied to all atoms[9]. The patterns of systematic absences observed in the data were consistent with either of the space groups *C2/m*, *C2* or *Cm*. The centrosymmetric space group *C2/m* was selected as the starting point and was confirmed by the successful solution and refinement of the structure. The structure was solved by a combination of direct methods (MITHRIL) and difference Fourier syntheses. Full matrix least-squares refinements minimized the function: $\Sigma_{hkl}\ w(|F_o|-|F_c|)^2$, where $w = 1/\sigma(F_o)^2$, $\sigma(F_o) = \sigma(F_o^2)/2\ F_o$ and $\sigma(F_o^2) = [\sigma(I_{raw})^2 + (0.02\ I_{net})^2]^{1/2}/Lp$. All metal atoms were refined with anisotropic thermal parameters. All oxygen atoms were refined with isotropic thermal parameters. Attempts to refine the Fe/Ti occupancy in the transition metal sites revealed no preferences in any of the metal sites, and a fixed disorder model with a completely random occupancy of the Fe and

Ti in the transition metal sites was used in the final refinements. Further details of the crystal structure investigations are available from the Fachinformationszentrum Karlsruhe, D-76344 Eggenstein-Leopoldshafen (Germany), on quoting the depository number CSD-59323.

Magnetic Measurements: Magnetic moments for polycrystalline samples were obtained by using a Quantum Design SQUID magnetometer. Variable temperature measurements in the range 5–700 K were made on a 80.2 mg sample mounted in a quartz sample holder. Magnetization vs. field loops were measured at T = 290 K at fields between −20 and +20 kOe on a smaller amount of sample (1.6 mg loaded in a gelatine capsule) to prevent from saturation of the SQUID signal. Data were corrected for the effects of the sample holders and for ionic diamagnetism assuming the $(Ba^{2+})_3(Fe^{3+})_{24}(Ti^{4+})_7(O^{2-})_{53}$ charge balance ($\chi_{dia} = -940 \times 10^{-6}$ emu/mol)[10].

[1] G. Bate in *Magnetic Oxides* (Ed.: D. J. Craik) John Wiley & Sons, London, **1975**, Ch. 12, p. 689.

[2] R. A. McCurrie, *Ferromagnetic Materials, Structure and Properties*, Academic Press, London, **1994**.

[3] [3a] X. Batlle, X. Obradors, J. Rodriguez-Carvajal, M. Pernet, M. V. Cabanas, M. Vallet, *J. Appl. Phys.* **1991**, *70*, 1614. – [3b] M. V. Cabanas, J. M. González-Calbet, J. Rodriguez-Carvajal, M. Vallet-Regí, *J. Solid State Chem.* **1994**, *111*, 229. – [3c] O. Kubo, T. Ido, H. Yokoyama, Y. Koike, *J. Appl. Phys.* **1985**, *57*, 4280. – [3d] Y. K. Hong, Y. J. Paig, D. G. Agresti, T. D. Shelfer, *J. Appl. Phys.* **1987**, *61*, 3872. – [3e] F. Chou, X. Feng, J. Liu, Y. Liu, *J. Appl. Phys.* **1987**, *61*, 3881. – [3f] L. Kalvoda, M. Dlouhá, S. Vratislav, Z. Jirák, *J. Magn. Magn. Mat.* **1990**, *87*, 243.

[4] [4a] T. A. Vanderah, Q. Huang, W. Wong-Ng, B. C. Chakoumakos, R. B. Goldfarb, R. G. Geyer, J. Baker-Jarvis, R. S. Roth, A. Santoro, *J. Solid State Chem.* **1995**, *120*, 121. – [4b] R. D. Adams, M. Danot, R. Layland, C. Payen, *Polyhedron* **1996**, *15*, 2567.

[5] I. E. Grey, A. Coulomb, X. Obradors, *J. Solid State Chem.* **1991**, *93*, 131.

[6] [6a] F. Habrey, M. Velicescu, *Acta Cryst.* **1974**, *B30*, 1507. – [6b] X. Obradors, A. Collomb, J. Pannetier, A. Isalgu; J. Tejada, J. C. Joubert, *Mat. Res. Bull.* **1983**, *18*, 1543.

[7] R. D. Adams, R. Layland, C. Payen, *Chem. Mater.* **1995**, *7*, 2168.

[8] [8a] G. Heimke, *Z. Angew. Phys.* **1963**, *15*, 271. – [8b] R. K. Tenzer, *J. Appl. Phys.* **1965**, *36*, 1180. – [8c] R. K. Tenzer, *J. Appl. Phys.* **1963**, *34*, 1267. – [8d] M. V. Cabanas, J. M. González-Calbet, M. Labeau, P. Mollard, M. Pernet, M. Vallet-Regí, *J. Solid State Chem.* **1992**, *101*, 265.

[9] *International Tables for X-ray Crystallography*, Kynoch Press: Birmingham, England, 1975; Vol. IV: (a) Table 2.2B, pp. 99–101; (b) Table 2.3.1; pp. 149–150.

[10] L. N. Mulay, E. A. Boudreaux, *Theory and Application of Molecular Diamagnetism*; Wiley-Interscience: New York, **1976**.

[96112]